J Solid State Electrochem (2012) 16:3171–3177
DOI 10.1007/s10008-012-1747-y

ORIGINAL PAPER

Synthesis of mesoporous NiO nanosheet and its application on mercury (II) sensor

Zhengcui Wu · Lidan Jiang · Yanan Zhu · Chengrong Xu · Yin Ye · Xiuhua Wang

Received: 3 January 2012 / Revised: 27 March 2012 / Accepted: 8 April 2012 / Published online: 8 May 2012

Abstract NiO nanosheets with uniformly distributed mesoporosity were successfully synthesized on a large scale by calcination of β-$Ni(OH)_2$ nanosheet precursor, which was simply prepared using 1,6-hexanediamine-assisted solution approach. The as-prepared mesoporous NiO nanosheets have been introduced for the first time for the sensing of mercury ions, which were found to be useful for selective electrochemical detection of Hg^{2+} with a linear range of 0.8 to 500 μM in pH 6.0 phosphate-buffered solutions, providing us another opportunity for exploring new electrochemical application of NiO nanomaterials.

Keywords NiO · Nanosheet · Mesoporosity · Hg^{2+} · Sensor

Introduction

Over the last decade, there has been a considerable interest in trace detection of heavy metal ions especially Hg^{2+} in aquatic ecosystems due to its threat in the environment and the severe effects on human health even in very low concentrations. As mercury can accumulate in the vital organs and tissues to bind with sulfur-containing proteins and enzymes, some important cell functions are inactivated which lead to a wide variety of diseases [1]. Therefore, it is highly desirable to develop simple and practical assays to detect Hg^{2+}. There have been numerous reports on optical Hg^{2+} detection by using Hg^{2+}-sensitive fluorophores or chromophores. However, most of these methods rely on optical techniques, such as colorimetry [2–4], fluorescence [5–7], and fluorescence polarization [8]. Compared with an optical instrument, electrochemical devices are relatively cost-effective and miniaturizable, so they are very attractive for trace analysis of heavy metals with high sensitivity, selectivity, short analysis time, and low power consumption, making electrochemical method being emerged as a preferable alternative [9–23].

Recent trends in development of biosensors have increasingly emphasized on the application of various nanomaterials to improve their analytical performance due to their small size, large surface area, high surface reaction activity, high catalytic efficiency, and corresponding potential electronic and chemical properties [24]. As for electrochemical sensors of Hg^{2+}, some of the recent research papers are focused on electrochemical detection using gold nanoparticles (AuNPs) with biomolecular modification, such as self-assembling AuNPs with urease modification [9], AuNP-based thymine–Hg^{2+}–thymine complexes [10], AuNP-based DNA probe [11], AuNP-based oligonucleotide [12], and amino acid-functionalized AuNPs [13]. Other research papers include AuNPs/carbon nanotube composites [14], AuNP–graphene hybrid nanocomposite [15], three-dimensional gold micro-/nanopore arrays containing 2-mercaptobenzothiazole [16], bimetallic Au-Pt nanoparticles/organic nanofibers [17], 5-mercapto-1-methyl-1-H-tetrazole functionalized silica films [18], multiwalled carbon nanotubes-ionic liquid-carbon paste electrode [19], and thiol functionalized chitosan-multiwalled carbon nanotubes nanocomposite film electrode [20]. Only a few examples of metal oxide nanomaterials for detection of Hg^{2+} have been reported [21–23]. Considering their

Electronic supplementary material The online version of this article (doi:10.1007/s10008-012-1747-y) contains supplementary material, which is available to authorized users.

Z. Wu (✉) · L. Jiang · Y. Zhu · C. Xu · Y. Ye · X. Wang (✉)
Anhui Key Laboratory of Molecule-Based Materials, Anhui Key Laboratory of Functional Molecular Solids, College of Chemistry and Materials Science, Anhui Normal University, Wuhu 241000, People's Republic of China
e-mail: zhengcui@mail.ahnu.edu.cn
e-mail: hua334@mail.ahnu.edu.cn

potentially good electrochemical properties with easily controlled sizes and morphologies at low cost, it is of great significance to develop electrochemical sensors based on metal oxide nanomaterials for selective detection of Hg^{2+} in low concentrations. Nickel oxide (NiO), as one of the most important transition metal oxides with environment-friendly nature, has received increasing attention due to its extensive applications, especially as a catalyst [25], lithium ion battery's electrode materials [26], antimicrobial agents [27], supercapacitor electrodes [28–31], and toxic gas sensor [32]. Recently, porous materials have received broad attention due to their fascinating properties, such as high specific surface area for adsorption, dense activated sites for interaction, and multiple tunnels for diffusion and transfer. Nanostructural porous materials have been of particular interest because of their enhanced performance compared with their bulk counterparts. There have been great efforts for the synthesis of different NiO porous nanostructures including porous nano/microspheres [29], hollow microspheres and tubular [30], nanoslices, nanoplates, and nanocolumns [31], nanoflakes [32], nanosheets [33], nanofibers [34], and ordered mesoporous NiO [35]. It has been shown that the electrochemical performance of NiO nanocrystals largely depends on its microstructure, surface area, and the presence of dopants [35–39], suggesting that the development of controlled syntheses of NiO nanostructures with the desired features, e.g., high electronic conductivity, low diffusion resistance to protons/cations, and high electroactive area, is of paramount importance [31]. In this paper, we designed an electrochemical sensor based on mesoporous NiO nanosheets and chitosan (CH) composite system for detection of Hg^{2+}, which exhibits higher catalytic effect on Hg^{2+} than CuO sub-microstructures that we recently reported [22]. The proposed method is simple, fast, reproducible, and cost-effective for the electrochemical determination of Hg^{2+}. Moreover, high sensitivity and selectivity, even at low concentrations, could be obtained. To the best of our knowledge, there is no report before on the design of a glassy carbon electrode based on NiO nanocomposite system for mercury determination. Therefore, it was our motivation to construct such nanocomposite electrode to reach higher sensitivity, selectivity, and also lower detection limit for Hg^{2+} determination, providing us another opportunity for exploring new electrochemical application of NiO nanomaterials.

Experimental

Reagents and apparatus

All of the chemical reagents were of analytical grade and used as received without any further purification. To study the electrochemical property of the product, stock solution of $HgCl_2$ was prepared by directly dissolving $HgCl_2$ in double distilled water. Phosphate buffer solutions (0.10 M) with various pH values from 5.0 to 7.5 were prepared with Na_2HPO_4, NaH_2PO_4, and KCl. All solutions were prepared with double distilled water.

Electrochemical experiments were performed with CHI660B electrochemical analyzer (ChenHua Instruments Co. Ltd., Shanghai, China) with a conventional three-electrode cell. The working electrode was as-prepared mesoporous NiO nanosheets-CH modified glassy carbon electrode (NiO-CH/GCE). A Hg/Hg_2Cl_2 (saturated KCl) and a platinum wire electrode were used as the reference and the auxiliary electrode, respectively. Prior to each experiment, solutions were purged with purified nitrogen for 15 min to remove oxygen and maintained under a nitrogen atmosphere during the course of the electrochemical experiment.

Synthesis and characterization of mesoporous NiO nanosheets

In a typical synthesis, 1 mmol of $NiC_2H_6O_4{\cdot}4H_2O$ was dissolved in 30 mL of distilled water under constant stirring, followed by the addition of 3 mL of 1,6-hexanediamine which was preliminarily melted at 50 °C in an oven. Then, the solution was loaded into a 50-mL Teflon-lined stainless steel autoclave and maintained at 150 °C for 12 h, and allowed to cool to room temperature naturally. The green precipitate was collected by centrifugation and washed with distilled water and ethanol for several times and then dried in a vacuum at 40 °C for 12 h. Afterward, the product was placed in a crucible and carefully heated up from room temperature to 400 °C at the rate of 5 °C/min and then maintained at 400 °C for 1 h in air. Finally, the product was collected.

X-ray powder diffraction (XRD) patterns of the products were recorded on a Shimadzu XRD-6000 X-ray diffractometer at a scanning rate of 0.05 s^{-1} with a 2θ range from 10° to 70°, with high-intensity Cu Kα radiation (λ=0.154060 nm). Field emission scanning electron microscope (FESEM) images were obtained on a Hitachi S-4800 field emission scanning electron microscope operated at an accelerating voltage of 5.0 kV. Transmission electron microscopy (TEM) analysis was used JEOL 2010 with an accelerating voltage of 200 kV. Brunauer–Emmett–Teller (BET) nitrogen adsorption–desorption was measured using a Micromeritics ASAP 2020 accelerated surface area and porosimetry system. Thermal gravimetric analysis (TGA) of the as-synthesized sample was carried out on a Shimadzu DTG-60A thermal analyzer at a heating rate of 10 °C/min from room temperature to 400 °C in air.

Electrode modification

The modified electrode was prepared as we previously reported [22]. Brifly, CH (50 mg) was dissolved in solution of 0.5 % HAc (10 mL) under stirring, and then mesoporous

NiO nanosheets (10 mg) were dissolved in chitosan solution. Next, 10 μL of the NiO-CH solution was dropped onto the surface of cleaned GCE and dried in air. The other modified electrodes were similarly prepared as above.

Results and discussion

Characterization of the product

The morphology and size of as-prepared precursor were first characterized with FESEM. Figure 1a displays a panoramic FESEM image of the precursor prepared by 1,6-hexanediamine-assisted solution approach, which shows the sample as large-scale nanosheets with an average length of 30–45 nm and width of 45–65 nm. Figure 1a shows that the product which consists entirely of such nanosheet structures with almost 100 % high yield can be easily achieved with this simple and easily controlled approach. The corresponding TEM image in Fig. 1b further clearly identified the nanosheet structures of the sample. The XRD pattern in Fig. 2a shows the diffraction peaks of the hexagonal phase of β-$Ni(OH)_2$ (JCPDS card, no. 74–2075) with lattice parameters of a= 3.136 Å and c=4.620 Å, suggesting the high crystallinity and high purity of the product.

The following calcination process was designed to create the porosity on the nanosheets. As expected, mesoporous NiO nanosheets have been prepared via calcining β-$Ni(OH)_2$ nanosheet precursor. Figure 2b shows the XRD pattern of the as-obtained product after calcination, and the diffraction peaks are in good agreement with the standard XRD pattern of the pure cubic phase of NiO (JCPDS card, no. 73–1523) with lattice parameters of a=4.180 Å, indicating that the pure phase of NiO can be obtained by calcining β-$Ni(OH)_2$ precursor. FESEM and TEM images of the calcination product are shown in Fig. 1c–e. The FESEM image in Fig. 1c indicates that the as-obtained NiO sample basically remains in a sheet-like morphology with a smaller size, average length of 25–40 nm and width of 40–60 nm, compared with that of the precursor before calcination, indicating a little shrinkage of the product after calcination. As seen from the TEM images in Fig. 1d and e, the honeycomb-like mesoporous nanostructures on the nanosheets were clearly presented, and the diameter of the mesoporosity was about 4–10 nm.

Such NiO nanosheets possess mesoporous structures also evidenced by the nitrogen sorption experiment (Fig. 3). The isotherm of the sample can be categorized as type IV, with a distinct hysteresis loop observed in the range of 0.45–1.0 P/P_0. The measurement shows that the BET surface area is 67.4 m^2/g, which is higher than that of nanoplates (20.2 m^2/g) and nanoslices (11.4 m^2/g) [31], and compares favorably with hollow tubular (69 m^2/g) [30], and there are two porous central distributions, one at 5.2 nm and the other at 31.5 nm (Fig. 3, inset), which are due to the mesoporosity in NiO nanosheets and the irregular packing of nanosheets. Such porous structure provides efficient transport pathways, leading to high accessibility and adsorptivity of Hg^{2+}, enhancing the sensing functionality in terms of the sensitivity.

TGA was carried out in air to analyze the dehydration process of the β-$Ni(OH)_2$ precursor. The TGA curve of the sample shows a weight loss of 17.6 % related to the procedure of dehydration [Electronic supplementary material (ESM) Fig. S1] that is believed to correspond to the release of water in the crystals, close to the theoretical calculations (19.4 %) according to the stoichiometry.

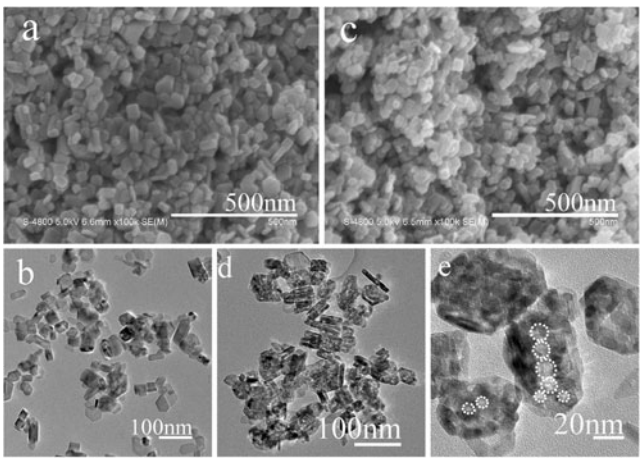

Fig. 1 FESEM and TEM images of as-prepared β-$Ni(OH)_2$ nanosheets and mesoporous NiO nanosheets. **a**, **b** FESEM image and TEM image of the β-$Ni(OH)_2$ nanosheets. **c**–**e** FESEM image and TEM images of the mesoporous NiO nanosheets. The *dotted circles* in (**e**) are used to highlight the mesopores in the NiO nanosheets

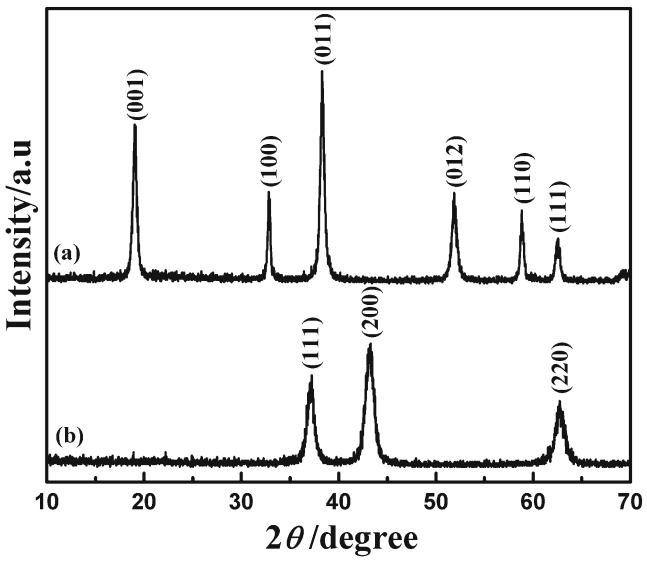

Fig. 2 XRD patterns of **a** the β-$Ni(OH)_2$ nanosheets and **b** the mesoporous NiO nanosheets

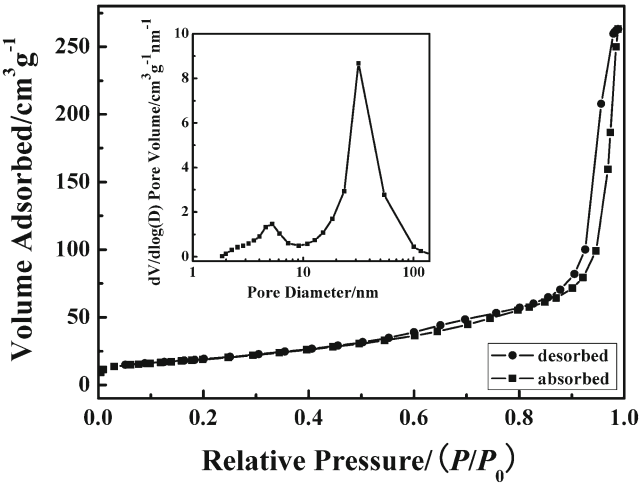

Fig. 3 Nitrogen adsorption–desorption isotherm of the mesoporous NiO nanosheet sample. The *inset* is its BJH pore-size distribution curve

Electrochemical activity of the Hg^{2+} on NiO-CH/GCE

Cyclic voltammetry (CV) was a useful tool to evaluate the performance of NiO-CH/GCE. Figure 4 showed the CVs of the different modified electrode recorded in 0.1 M phosphate-buffered solutions (pH=6.0) in the presence of 20 μM Hg^{2+}. There was a faintness oxidation peak occurring at voltammetric curves using bare GCE (Fig. 4 curve a) but not had homologous reduction peak scanning between 0.4 and –0.4 V. This result indicated that the electrochemical process of Hg^{2+} on bare GCE was hard and irreversible. On CH/GCE, the oxidation current increased obviously (Fig. 4 curve b), but still not had homologous reduction peak. While on β-$Ni(OH)_2$-CH/GCE, NiO/GCE, or NiO-CH/GCE (Fig. 4 curve c–e), not only the oxidation peak current increased and slightly shifted positively to 0.15 V but also the reduction peak was present at 0.06 V. The electrochemical process of Hg^{2+} on β-$Ni(OH)_2$-CH/GCE, NiO/GCE, and NiO-CH/GCE was quasi-reversible, while on NiO-CH/GCE, the oxidation peak and reduction peak increased greatly, demonstrating that the composite of mesoporous NiO nanosheets and chitosan had best catalytic role to Hg^{2+}. It was conjectured that the chemical compositions of the β-$Ni(OH)_2$ and NiO nanosheets that have adsorption ability toward Hg (II) made them have good response to Hg^{2+}, and the mesoporous structure of the NiO nanosheets developing a larger surface area enabled the larger adsorption capacity, improving its sensing performance in practical applications, which is similar with γ-AlOOH(boehmite) @SiO_2/Fe_3O_4 porous magnetic microspheres for detection of toxic metal ions in drinking water [21].

In order to study the interface properties of surface-modified electrode, electrochemical impedance spectroscopy (EIS) was done. In electrochemical impedance spectroscopy, the impedance spectrum includes a semicircle portion at high frequencies corresponding to the electron transfer-limited process and a linear part at the low frequencies resulting from the diffusion-limited electrochemical process. The semicircle diameter of EIS equals the electron transfer resistance (R_{et}). This resistance exhibited the electron transfer resistance of the modified layer, which showed its blocking behavior of the electrode. The increase or decrease in its value exactly characterized the modification of electrode surface [40]. ESM Fig. S2 exhibits the impedance spectroscopies of different electrodes. After the β-$Ni(OH)_2$ nanosheets or the mesoporous NiO nanosheets and chitosan were modified onto the GCE (curve a and b), the semicircle diameter of EIS, R_{et}, increased compared with the bare glassy carbon electrode (curve c), and the impedance changes of the modification process showed that the as-prepared nanomaterials had attached to the electrode surface. At the same time, the R_{et} is different when different nanomaterials modified onto the glassy carbon electrode. The R_{et} of the β-$Ni(OH)_2$ nanosheets is larger than that of the mesoporous NiO nanosheets, which meant that the electron transfer ability of the mesoporous NiO nanosheets is larger than that of the β-$Ni(OH)_2$ nanosheets. The modification using different materials could be further confirmed using cyclic voltammograms of $Fe(CN)_6^{3-/4-}$ (ESM Fig. S3). It is clear that a decrease in the amperometric response and an increase in the peak-to-peak separation between the cathodic and anodic waves of the redox probe compared to that of GCE after modification using the NiO-CH and β-$Ni(OH)_2$-CH, accounting for the electron

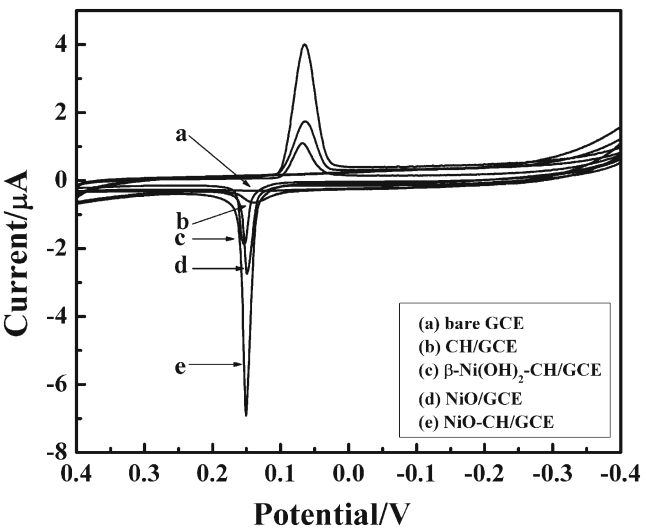

Fig. 4 Cyclic voltammograms of 20 μM Hg^{2+} on *a* bare GCE, *b* CH/GCE, *c* β-$Ni(OH)_2$-CH/GCE, *d* NiO/GCE, and *e* NiO-CH/GCE in phosphate buffer solutions (pH=6.0). Scan rate, 100 mV s^{-1}

transfer kinetics of $Fe(CN)_6^{3-/4-}$, are gradually obstructed. It demonstrates that the electron transfer ability of the mesoporous NiO nanosheets is larger than that of the β-$Ni(OH)_2$ nanosheets from another point of view. The reason may be attributed to the better conductivity of the NiO nanomaterials and the fact that the mesoporous NiO nanosheets has not only larger surface but also more electron transfer passage than that of the β-$Ni(OH)_2$ nanosheets, which led to the probe arriving to the surface of the electrode easily. The result consisted of the EIS of different modified electrodes.

The morphology and porosity of NiO material on the catalytic redox of mercury were also examined. The flower-like porous NiO structure with larger mesoporosity was obtained by calcination of flower-like α-$Ni(OH)_2$ (ESM Fig. S4). Because α-$Ni(OH)_2$ is a hydroxyl-deficient phase which consists of stacks of positively charged $Ni(OH)_{2-x}$ layers and contains intercalated anions and water molecules in the interlayer space to restore charge neutrality, it undergoes multistep and larger mass losses in the thermogravimetric experiment compared with the β-hydroxide phase due to the decomposition of the intercalated anions (ESM Fig. S5), leading to larger mesoporosity on the final NiO nanostructures. The mesoporosity can be clearly seen on the SEM image of ESM Fig. S4. The CV of the mesoporous flower-like NiO-modified electrode recorded in 0.1 M phosphate-buffered solution (pH=6.0) in the presence of 20 μM Hg^{2+} has been done, and the currents of the oxidation peak and reduction peak were smaller compared with that of mesoporous NiO nanosheets (ESM Fig. S6), which may be due to the lower surface area of the porous NiO flower related to the larger pore diameters.

The effect of the solution pH on electrochemical behaviors of Hg^{2+} on the current response for 20 μM Hg^{2+} at NiO-CH/GCE was examined in 0.1 M PBS at various pH values ranging from 5.5 to 7.5. The result showed that the anodic peak current reached the highest at pH=6.0 (ESM Fig. S7). Therefore, pH 6.0 was the most appropriate for Hg^{2+} redox on NiO-CH/GCE.

Differential pulse voltammetry of NiO-CH/GCE

According to the above experimental results, it has been found there was excellent electron transfer appearance between the mesoporous NiO nanosheets and Hg^{2+}, suggesting that the modified electrode could be applied to the determination of Hg^{2+}. In order to obtain the liner range of detection, we further used differential pulse voltammetry (DPV) to evaluate the performance of the sensor. Figure 5 showed the DPV (at 0.092 V) of the as-prepared NiO-CH/GCE sensor to the successive addition of Hg^{2+} in PBS (pH=6.0). The peak current (I_p) linearly increased with the

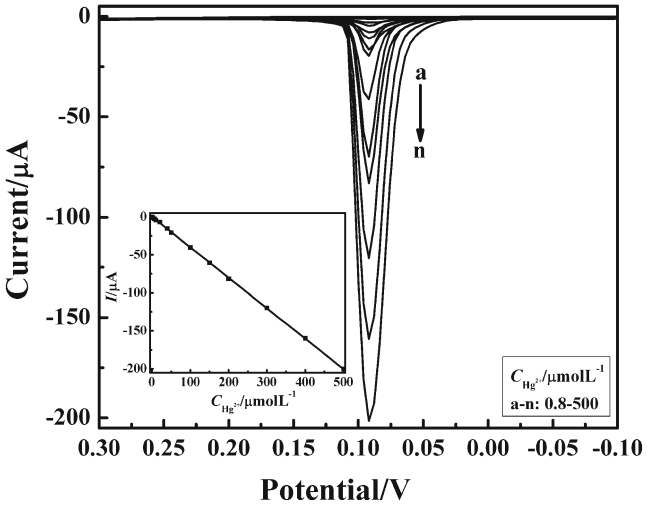

Fig. 5 DPV of NiO-CH/GCE upon successive additions of 1.2 μM (*b*), 4 μM (*c*, *d*), 10 μM (*e*→*h*), 50 μM Hg^{2+} (*i*→*k*), and 100 μM Hg^{2+} (*l*→*n*), respectively (curve *a* with 0.8 μM Hg^{2+} in PBS (pH=6.0)). *Inset* the relationship between the concentration of Hg^{2+} and the anodic peak current (I_p)

increase in concentration (*c*). A plot of I_p versus *c* was shown in the inset of Fig. 5, which yielded good linearity, and the linear equation is $y=-0.40046x-0.10262$ (*x*, the concentration of the Hg^{2+}, micromolars; *y*, the anodic peak current, microamperes), with a correlation coefficient of 0.9998. As expected from the DPV data, NiO-CH/GCE showed a good linear response to the changes of Hg^{2+} concentration in the range from 0.8 to 500 μM. Based on signal to noise ratio of 3, the limit of detection was established to be 0.04 μM. This is better than or compares favorably with other reported electrodes [41, 42], also better than CuO sub-microstructure sensor that we recently reported [22], showing our method was effective in the determination of low concentration of Hg^{2+} in sample.

Stability, reproducibility, anti-interferences, and application for sample analysis of the sensor

The outstanding advantages of the NiO-CH/GCE are its good stability, acceptable reproducibility, and excellent selectivity. After 30 consecutive cyclic scans, the CV at NiO-CH/GCE achieved a steady state and kept almost unchanged. When the electrode was stored in air at ambient conditions for 20 days, the current still retained 97 % of its initial response to Hg^{2+}, showing an excellent stability. The NiO-CH/GCE electrode showed a relative standard deviation of 4 % for ten successive assays with 20 μM Hg^{2+} and 3 % for six determinations based on six same fabrications of the modified electrode. Hence, the electrode has an acceptable reproducibility. The long-term stability and the good reproducibility of the sensor were desirable for most routine analysis.

Under optimized experimental conditions mentioned above, the possible interferences of other metal ions like Cd^{2+}, Cr^{3+}, Zn^{2+}, Pb^{2+}, Fe^{3+}, Fe^{2+}, Cu^{2+}, which are common existing interfering species in the real samples for the determination of 20 μM Hg^{2+}, were examined with mesoporous NiO-CH-modified electrode. The DPV selectivity experiment of the electrode towards the addition of 20 μM Hg^{2+} and 100 μM Cd^{2+}, 200 μM Cu^{2+}, and 500 μM each of Cr^{3+}, Zn^{2+}, Pb^{2+}, Fe^{3+}, Fe^{2+} ions was examined (ESM Fig. S8). As can be seen in ESM Fig. S8, the peak currents belonging to Cd^{2+} and Cu^{2+} appeared separately, while that of other interference ions did not appear, and the peak current of Hg^{2+} has no obvious change, indicating that the above metal ions did not interfere in the determination of Hg^{2+}.

To evaluate the performance of NiO-CH-modified electrode in a real sample, an analysis of tap water was carried out using the standard addition method. Standard solutions of Hg (II) were added to tap water containing 20 μM Hg^{2+} for quantitative determination of Hg (II). The DPV parameters were the same as used previously. The results obtained on tap water showed ±8 % deviation. Considering the excellent measurement stability, such a material holds great potential for detection of Hg^{2+} in real samples.

Conclusion

In summary, mesoporous NiO nanosheets have been successfully prepared by calcination of β-$Ni(OH)_2$ nanosheet precursor, which was simply synthesized using 1,6-hexanediamine-assisted solution approach. A natural polymer, chitosan, has been used as a dispersant to fabricate a Hg^{2+} sensor based on mesoporous NiO nanosheets. Compared to β-$Ni(OH)_2$/GCE, NiO-CH/GCE displayed higher electrocatalytic activity towards the redox of Hg^{2+}, which may be attributed to better conductivity, larger special surface, and more electron transfer passage of mesoporous NiO nanosheets, which led to the probe arriving to the surface of the electrode easily. The result demonstrated NiO-CH/GCE exhibited the prominent activity for redox of Hg^{2+}, and it gave a good stability, reproducibility, and anti-interferences, which could be used as an effective amperometric sensor for the determination of low concentration of Hg^{2+} in sample.

Acknowledgments We thank Prof. Dr. Feng Gao and Dr. Huamao Chen of Anhui Normal University for their good suggestions in the analysis of the results and Dr. Yan Xue of the University of Science and Technology of China for her help in the BET measurement of the sample. This work was financially supported by the Natural Science Foundation of Anhui Province (11040606M32), Natural Science key Foundation of Anhui Province Education Administration (KJ2010A144), Innovation Foundation of Anhui Normal University (2011cxjj10 and 2011cxjj11), Innovation Experimental Program for College Student of Anhui Normal University (cxsy11083), and the Startup Foundation for Doctor of Anhui Normal University.

References

1. Harris HH, Pickering IJ, George GN (2003) Science 301:1203–1203
2. Hu KC, Lan DX, Li XM, Zhang SS (2008) Anal Chem 80:9124–9130
3. Lee JS, Han MS, Mirkin CA (2007) Angew Chem Int Ed 46:4093–4096
4. Wang H, Wang YX, Jin JY, Yang RH (2008) Anal Chem 80:9021–9033
5. Lee JS, Mirkin CA (2008) Anal Chem 80:6805–6808
6. Chiang CK, Huang CC, Liu CW, Chang HT (2008) Anal Chem 80:3716–3721
7. Liu J, Lu Y (2007) Angew Chem Int Ed 46:7587–7590
8. Ye BC, Yin BC (2008) Angew Chem Int Ed 47:8386–8389
9. Yang YH, Wang ZJ, Yang MH, Guo MM, Wu ZY, Shen GL, Yu RQ (2006) Sensor Actuator B 114:1–8
10. Miao P, Liu L, Li Y, Li GX (2009) Electrochem Commun 11:1904–1907
11. Liu XP, Sun CH, Wu HW, Zhang YF, Jiang JH, Shen GL, Yu RQ (2010) Electroanalysis 22:2110–2116
12. Zhu ZQ, Su YY, Li J, Li D, Zhang J, Song SP, Zhao Y, Li GX, Fan CH (2009) Anal Chem 81:7660–7666
13. Safavi A, Farjami E (2011) Anal Chim Acta 688:43–48
14. Xu H, Zeng LP, Xing SJ, Shi GY, Xian YZ, Jin LT (2008) Electrochem Commun 10:1839–1843
15. Gong JM, Zhou T, Song DD, Zhang LZ (2010) Sensor Actuator B 150:491–497
16. Fu XC, Chen X, Guo Z, Kong LT, Wang J, Liu JH, Huang XJ (2010) Electrochim Acta 56:463–469
17. Gong JM, Zhou T, Song DD, Zhang LZ, Hu XL (2010) Anal Chem 82:567–573
18. Sanchez A, Walcariusa A (2010) Electrochim Acta 55:4201–4207
19. Khani H, Rofouei MK, Arab P, Gupta VK, Vafaei Z (2010) J Hazard Mater 183:402–409
20. Deng WF, Tan YM, Li YY, Wen YQ, Su ZH, Huang Z, Huang SQ, Meng Y, Xie QJ, Luo YP, Yao SZ (2010) Microchim Acta 169:367–373
21. Wei Y, Yang R, Zhang YX, Wang L, Liu JH, Huang XJ (2011) Chem Commun 47:11062–11064
22. Wu ZC, Jiang LD, Chen HM, Xu CR, Wang XH (2012) J Mater Sci Mater Electron 423:858–864
23. Yin ZJ, Wu JJ, Yang ZS (2010) Microchim Acta 170:307–312
24. Miao XM, Yuan R, Chai YQ, Shi YT, Yuan YY (2008) J Electroanal Chem 612:157–163
25. Wang Y, Zhu J, Yang X, Lu L, Wang X (2005) Thermochim Acta 437(1–2):106–109
26. Needham SA, Wang GX, Liu HK (2006) J Power Sources 159:254–257
27. Pang H, Lu Q, Li Y, Gao F (2009) Chem Commun 48:7542–7544
28. Xu J, Gao L, Cao JY, Wang WC, Chen ZD (2011) J Solid State Electrochem 15:2005–2011
29. Yuan CZ, Zhang XG, Su LH, Gao B, Shen LF (2009) J Mater Chem 19:5772–5777
30. Song X, Gao L (2008) J Phys Chem C 112:15299–15305
31. Zhang XJ, Shi WH, Zhu JX, Zhao WY, Ma J, Mhaisalkar S, Maria TL, Yang YH, Zhang H, Hng HH, Yan QY (2010) Nano Res 3 (9):643–652
32. Lang JW, Kong LB, Wu WJ, Luo YC, Kang L (2008) Chem Commun 35:4213–4215

33. Hoa ND, El-Safty SA (2011) Chem Eur J 17:12896–12901
34. Qiu YJ, Yu J, Zhou XS, Tan CL, Yin J (2009) Nanoscale Res Lett 4:173–177
35. Jiao F, Hill AH, Harrison A, Berko A, Chadwick AV, Bruce PG (2008) J Am Chem Soc 130:5262–5266
36. Yuan CZ, Gao B, Zhang XG (2007) J Power Sources 173:606–612
37. Xing W, Li F, Yan ZF, Lu GQ (2004) J Power Sources 134:324–330
38. Yan HW, Blanford CF, Holland BT, Parent M, Smyrl WH, Stein A (1999) Adv Mater 11:1003–1006
39. Wei TY, Chen CH, Chien HC, Lu SY, Hu CC (2010) Adv Mater 22:347–351
40. Pei RJ, Cheng ZL, Wang EK, Yang XR (2001) Biosens Bioelectron 16:355–361
41. Vinod KG, Sudeshna C, Heinrich L (2005) Talanta 66:575–580
42. Kuralay F, Ozyoruk H, Yıldız A (2007) Enzyme Microb Technol 40:1156–1159